

# SPECTRAL APPROACH TO THE SCATTERING MAP FOR THE SEMI-CLASSICAL DEFOCUSING DAVEY-STEWARTSON II EQUATION

CHRISTIAN KLEIN, KEN MCLAUGHLIN, AND NIKOLA STOILOV

ABSTRACT. The inverse scattering approach for the defocusing Davey-Stewartson II equation is given by a system of D-bar equations. We present a numerical approach to semi-classical D-bar problems for real analytic rapidly decreasing potentials. We treat the D-bar problem as a complex linear second order integral equation which is solved with discrete Fourier transforms complemented by a regularization of the singular parts by explicit analytic computation. The resulting algebraic equation is solved either by fixed point iterations or GMRES. Several examples for small values of the semi-classical parameter in the system are discussed.

## 1. INTRODUCTION

We present an efficient numerical approach to the direct and inverse scattering maps for the defocusing Davey-Stewartson (DS) II equation. The latter appears in many applications in nonlinear optics and hydrodynamics and can be written in the form

$$(1) \quad \begin{aligned} i\epsilon q_t + \frac{\epsilon^2}{2} (q_{xx} - q_{yy}) &= -|q|^2 q - \varphi q, \\ \varphi_{xx} + \varphi_{yy} &= -2(|q|^2)_{xx}. \end{aligned}$$

This equation is an integrable 2d generalisation of the nonlinear Schrödinger (NLS) equation [1]. Here  $\epsilon \ll 1$  is a small parameter similar to  $\hbar$  in the Schrödinger equation, and the limit  $\epsilon \rightarrow 0$  is accordingly called the semiclassical limit. Since the DS II equation is purely dispersive, in the semiclassical limit the solutions show zones of rapid modulated oscillations called *dispersive shock waves* (DSW), see for instance [9, 10].

The study of DSWs for generic dispersive partial differential equations (PDEs) is limited to multi-scales analysis for sufficiently small initial data. For completely integrable PDEs as the NLS equation, a more general description of DSWs can be given, see for instance [5, 4, 7, 12] and references therein. Since the DS II equation is completely integrable, see [1, 18], an approach similar to the treatment of NLS could be applied. A first step in this direction has been taken in [2].

The inverse scattering map for the defocusing DS II equation is given by the following elliptic system.

$$(2) \quad \epsilon \begin{pmatrix} \bar{\partial} & 0 \\ 0 & \partial \end{pmatrix} \psi = \frac{1}{2} \begin{pmatrix} 0 & q \\ \bar{q} & 0 \end{pmatrix} \psi, \quad \epsilon \ll 1.$$

The operators  $\partial$  and  $\bar{\partial}$  are defined via

$$\partial = \frac{1}{2} \left( \frac{\partial}{\partial x} - i \frac{\partial}{\partial y} \right), \quad \bar{\partial} = \frac{1}{2} \left( \frac{\partial}{\partial x} + i \frac{\partial}{\partial y} \right).$$

We note here that this system appears in a number of different applications, for instance in the context of further integrable partial differential equations [3], of 2D orthogonal polynomials, of Normal Matrix Models in Random Matrix Theory, see e.g. [8], and of electrical impedance tomography (EIT) [6, 14, 21]. The D-bar system appearing in the inverse scattering approach to the defocusing Davey-Stewartson II equation has the most general form (see [16] and references therein) and is hence the subject of this work.

---

*Date:* September 25, 2018.

*Key words and phrases.* D-bar problems, Fourier spectral method, Davey-Stewartson equations.

In all applications the quest is to recover a vector-valued solution  $\psi = \psi(z, k) = \begin{pmatrix} \psi_1 \\ \psi_2 \end{pmatrix}$  with the following asymptotic behaviour as  $|z| \rightarrow \infty$ :

$$\begin{aligned} \lim_{|z| \rightarrow \infty} \psi_1 e^{-kz/\epsilon} &= 1, \\ \lim_{|z| \rightarrow \infty} \psi_2 e^{-\bar{k}\bar{z}/\epsilon} &= 0, \end{aligned}$$

writing  $k = k_1 + ik_2$  for  $(k_1, k_2) \in \mathbb{R}^2$ , a complex-valued parameter playing the role of a spectral variable. The quantity  $\psi$  is referred to as a *complex geometric optics* (CGO) solution. Information relevant to the inverse problem at hand is obtained from the CGO solution by extracting the value at either 0 or  $\infty$ , both of which are delicate limits.

For the DSII equation, the *reflection coefficient*,  $r = r^\epsilon(k)$ , is encoded in the sub-leading term in the asymptotic expansion of  $\psi$  as  $z \rightarrow \infty$ , via

$$(3) \quad \psi_2 e^{-\bar{k}\bar{z}} = \frac{\bar{r}^\epsilon(k)}{2\bar{z}} + \mathcal{O}\left(\frac{1}{|z|^2}\right).$$

In fact, the notation  $r(k)$  does not imply that the function is holomorphic (and the same holds for any function of a complex variable in this paper), and what we have is a transformation from the potential  $q(x, y)$  (again a function of two real variables) to a function  $r(k_1, k_2)$ , which extends to Lipschitz continuous and invertible mapping on the function space  $L^2(\mathbb{C})$  (see [16, 15], and the references contained therein).

Now, if  $q = q(x, y, t, \epsilon)$  evolves according to the DSII equation (1), then the reflection coefficient evolves according to

$$r = r^\epsilon(k, t) = r^\epsilon(k, 0) e^{\frac{-it}{4\epsilon}(k^2 + \bar{k}^2)}.$$

In this sense, the mapping from  $q$  to  $r$  linearises the DSII flow. More amazingly, the inverse problem of reconstructing the potential  $q(x, y, t, \epsilon)$  from the reflection coefficient  $r(k, t)$  is also a D-bar problem, only in the complex variable  $k$ . Indeed, setting

$$(4) \quad \Phi_1 = \Phi_1^\epsilon(k; z, t) := e^{-kz/\epsilon} \psi_1 \quad \text{and} \quad \Phi_2 = \Phi_2^\epsilon(k; z, t) := e^{-\bar{k}\bar{z}/\epsilon} \psi_2,$$

it turns out that one has, for each  $z \in \mathbb{C}$ ,

$$(5) \quad \epsilon \bar{\partial}_k \Phi_1 = \frac{1}{2} e^{(\bar{k}\bar{z} - kz)/\epsilon} \overline{r^\epsilon(k, t)} \Phi_2, \quad \epsilon \partial_k \Phi_2 = \frac{1}{2} e^{-(\bar{k}\bar{z} - kz)/\epsilon} r^\epsilon(k, t) \Phi_1$$

where,

$$\bar{\partial}_k := \frac{1}{2} \left( \frac{\partial}{\partial k_1} + i \frac{\partial}{\partial k_2} \right), \quad \partial_k := \frac{1}{2} \left( \frac{\partial}{\partial k_1} - i \frac{\partial}{\partial k_2} \right),$$

and the asymptotic conditions

$$(6) \quad \lim_{|k| \rightarrow \infty} \Phi_1^\epsilon(k; z, t) = 1 \quad \text{and} \quad \lim_{|k| \rightarrow \infty} \Phi_2^\epsilon(k; z, t) = 0.$$

The functions  $\Phi_1$  and  $\Phi_2$ , being uniquely determined by the above elliptic system (5) and boundary conditions (6), yield the potential  $q(x, y, t, \epsilon)$  through the asymptotic behavior as  $|k| \rightarrow \infty$ :

$$\Phi_2 = \frac{\overline{q(x, y, t, \epsilon)}}{2k} + \mathcal{O}(|k|^{-2}).$$

In this paper we present a numerical method that is spectrally accurate to solve the D-bar equation (2) with the desired asymptotic conditions. The potential  $q = q(x, y)$  is assumed to be in the Schwartz class  $\mathcal{S}(\mathbb{R}^2)$  of rapidly decreasing smooth functions.

Knudsen, Mueller and Siltanen [13] developed a numerical approach to solving D-bar problems of the form

$$\bar{\partial} M = q(x, y) \bar{M}, \quad M = 1 + \mathcal{O}\left(\frac{1}{|z|}\right) \quad \text{as } |z| \rightarrow \infty.$$

They use Fourier techniques for these equations in an integral representation (see below). Their method is of first order since the singular integrand was regularized by putting it equal to zero where it diverges. In

[8] the authors present an enhanced version of this approach having spectral accuracy for potentials  $q(x, y)$  in the Schwartz class. They use this numerical method to compute the reflection coefficient  $r(k)$ , as well as the inverse problem of computing the potential  $q(x, y, t)$ , in the case that  $\epsilon = 1$ . (The numerical method is summarized in Section 2 below.) Subsequent to that, in [2], the asymptotic behavior of the DSII equation (1) with  $\epsilon \rightarrow 0$  is considered, along with a number of different numerical methods aimed at elucidating the challenges in the asymptotic analysis.

In this work we are interested in the numerical construction of CGO solutions to equation (2) for potentials  $q$  in the Schwartz class  $\mathcal{S}(\mathbb{R}^2)$  of rapidly decreasing smooth functions, with  $\epsilon$  tending to zero. The paper is organised as follows: In Section 2 we reformulate the D-bar problem as an integral equation and discuss the basic ingredients of our numerical implementation. In Section 3 we solve the discretised integral equation of the preceding section by a fixed point iteration, whereas in Section 4 we do the same by using the GMRES method. Finally, we draw our conclusions in Section 5.

## 2. INTEGRAL EQUATION AND NUMERICAL APPROACHES

In this section we present a reformulation of system (2), which is suited for an efficient numerical treatment and discuss the employed numerical approach.

**2.1. Integral equations.** The CGO solutions to (2) have an essential singularity at infinity which is numerically problematic for obvious reasons. The quantities  $\Phi_1$  and  $\Phi_2$  defined in (4), with asymptotic normalization (6), are well suited for numerical simulations. As stated in the introduction, in terms of these functions, system (2) takes the form

$$(7) \quad \begin{aligned} \epsilon \bar{\partial} \Phi_1 &= \frac{1}{2} q e^{(\bar{k}\bar{z} - kz)/\epsilon} \Phi_2, \\ \epsilon \partial \Phi_2 &= \frac{1}{2} \bar{q} e^{(kz - \bar{k}\bar{z})/\epsilon} \Phi_1. \end{aligned}$$

**Remark 2.1.** System (7) is related to the corresponding system with  $\epsilon = 1$  via the transformation  $q \mapsto q/\epsilon$  and  $k \mapsto k/\epsilon$ . Since we vary  $\epsilon$  in the examples, we will concentrate on potentials with  $\|q\|_\infty \sim 1$  (smaller values of  $\epsilon$  imply larger values of  $|q|$  in the system with  $\epsilon = 1$ ) and discuss only the cases  $k = 0$  and  $k = 1$ .

We define  $\xi = \xi_1 + i\xi_2$  where  $\xi_1$  and  $\xi_2$  are the dual Fourier variable to  $x$  and  $y$  respectively. The Fourier transform of a function  $\Phi$  is defined as

$$\begin{aligned} \hat{\Phi} &= \mathcal{F}\Phi := \frac{1}{2\pi} \int_{\mathbb{R}^2} \Phi e^{-i(\xi\bar{z} + \bar{\xi}z)/2} \Phi dx dy, \\ \Phi &= \mathcal{F}^{-1}\hat{\Phi} = \frac{1}{2\pi} \int_{\mathbb{R}^2} e^{i(\xi\bar{z} + \bar{\xi}z)/2} \hat{\Phi} d\xi_1 d\xi_2. \end{aligned}$$

This implies formally

$$\mathcal{F}(\bar{\partial}\Phi_1) = \frac{i}{2} \xi \hat{\Phi}_1, \quad \mathcal{F}(\partial\Phi_2) = \frac{i}{2} \bar{\xi} \hat{\Phi}_2.$$

Thus we get for the second relation in (7)

$$(8) \quad \Phi_2 = \mathcal{F}^{-1} \left[ \frac{1}{i\xi\epsilon} \mathcal{F}(\bar{q}\Phi_1) \circ (\xi - 2i\bar{k}/\epsilon) \right],$$

which is equivalent to

$$(9) \quad \Phi_2 = e^{(kz - \bar{k}\bar{z})/\epsilon} \mathcal{F}^{-1} \left[ \frac{1}{i\epsilon(\bar{\xi} - 2ik/\epsilon)} \mathcal{F}(\bar{q}\Phi_1) \right].$$

Therefore  $\Phi_2$  is given by a singular Fourier integral times an oscillatory term. An analogous formula can be obtained for  $\Phi_1$ ,

$$(10) \quad \Phi_1 = \mathcal{F}^{-1} \left[ \frac{1}{i\xi\epsilon} \mathcal{F}(q\Phi_2) \circ (\xi - 2i\bar{k}/\epsilon) \right].$$

Replacing in (10)  $\Phi_2$  via (9), one gets an integral equation for  $\Phi_1$ ,

$$(11) \quad \Phi_1 = -\mathcal{F}^{-1} \left\{ \frac{1}{\epsilon \xi} \mathcal{F} \left[ q \mathcal{F}^{-1} \left( \frac{\mathcal{F}(\bar{q}\Phi_1)}{\epsilon(\xi - 2ik/\epsilon)} \right) \right] \right\},$$

i.e., a singular integral equation for  $\Phi_1$  which, once discretised, can be solved iteratively either by GMRES or by a fixed point iteration. Remarkably, this equation does not contain oscillatory terms, and it is complex linear in  $\Phi_1$ . After obtaining a solution of this equation, the function  $\Phi_2$  follows from (9) via a singular integral.

**Remark 2.2.** System (2) can be written as a pure D-bar system by taking the complex conjugate of the second equation and by working with  $\bar{\psi}_2$  instead of  $\psi_2$ . Diagonalising the matrix on the resulting right hand side yields equations of the form ( $\mu_{\pm} := \psi_1 \pm \bar{\psi}_2$ )

$$\bar{\partial}\mu_{\pm} = \pm \frac{q}{2}\bar{\mu}_{\pm},$$

see for instance [8]. These equations are not complex linear and thus have to be split into real and imaginary part in order to apply the Krylov techniques [17] we will use in section 4. This essentially doubles memory requirements which makes the approach of the present paper much more efficient in this respect.

However, equation (11) is not ideal for a numerical treatment with discrete Fourier transforms, since the functions  $\Phi_{1,2}$  are not in the Schwarz class. Indeed, the singular Fourier symbols appearing in the equations (11) and (9) cause these functions to decay too slowly at  $\infty$ . But the function  $S$  defined by (essentially the Fourier transform of the D-bar derivative of  $\Phi_1$ )

$$(12) \quad S := \xi \hat{\Phi}_1, \quad \Phi_1 = \mathcal{F}^{-1} \left( \frac{S}{\xi} \right) + 1,$$

is in this class. Thus we will consider the equation following from (11),

$$(13) \quad S = -\mathcal{F} \left[ q \mathcal{F}^{-1} \left( \frac{1}{\epsilon(\bar{\xi} - 2ik/\epsilon)} \mathcal{F} \left\{ \frac{\bar{q}}{\epsilon} \left( \mathcal{F}^{-1} \left( \frac{S}{\xi} \right) + 1 \right) \right\} \right) \right].$$

The reflection coefficient (3) was discussed in detail in [8], here the focus is on the solutions to the D-bar system (2). Nevertheless, we note here that it can be obtained from a given solution  $\Phi_1$  in a straight forward way at essentially no additional computational cost. Note that the solution for  $\Phi_2$  in (7) can be written in terms of a solid Cauchy transform as

$$\Phi_2 = \frac{1}{\pi} \int_{\mathbb{R}^2} \frac{e^{(kz' - \bar{k}\bar{z}')/\epsilon} \bar{q} \Phi_1}{\epsilon(\bar{z} - \bar{z}')} dx' dy'$$

Thus we get with (3) by computing  $\lim_{|z| \rightarrow \infty} \bar{z} \Phi_2$

$$(14) \quad \bar{r}(k) = \frac{2}{\epsilon \pi} \int_{\mathbb{R}^2} e^{(kz - \bar{k}\bar{z})/\epsilon} \bar{q} \Phi_1 dx dy.$$

This, up to a multiplicative factor, corresponds to the Fourier transform of  $e^{kz - \bar{k}\bar{z}} \bar{q} \Phi_1$  for  $\xi = 0$ . Since we will work on a Fourier grid as detailed below, this integral can be computed simply as the mean value of the integrand on the grid thus providing a spectral method, see the discussion in [20]. For given  $\Phi_1$ , one just has to multiply the function with  $e^{kz - \bar{k}\bar{z}} \bar{q}$  and compute the mean value. For a potential in the Schwartz class, this approach is efficient even for large  $k$  since  $q$  is rapidly decreasing with  $|z|$  thus delimiting the effects of the oscillatory term  $e^{kz - \bar{k}\bar{z}}$ .

**2.2. Singular Fourier integrals.** The task is thus to compute two singular integrals, the first being  $\mathcal{F}^{-1}(S/\xi)$ . As in [8] we observe that  $2\mathcal{F}^{-1} \exp(-|\xi|^2) = \exp(-|z|^2/4)$  and thus

$$(15) \quad \mathcal{F}^{-1} \left( \frac{e^{-|\xi|^2}}{\xi} \right) = \frac{i}{z} \left( 1 - e^{-\frac{|z|^2}{4}} \right),$$

as well as

$$(16) \quad \mathcal{F}^{-1} \left( \frac{\bar{\xi}^n e^{-|\xi|^2}}{\xi} \right) = (-2i\partial)^n \frac{i}{z} \left( 1 - e^{-\frac{|z|^2}{4}} \right) =: \eta_n, \quad n = 0, 1, \dots$$

We show the first two functions  $\eta_0, \eta_1$  in Fig. 1. They vanish at the origin and have an annular structure. It can be seen that they are of order  $10^{-5}$ . The  $L^\infty$  norm of these functions decreases with  $n$ .

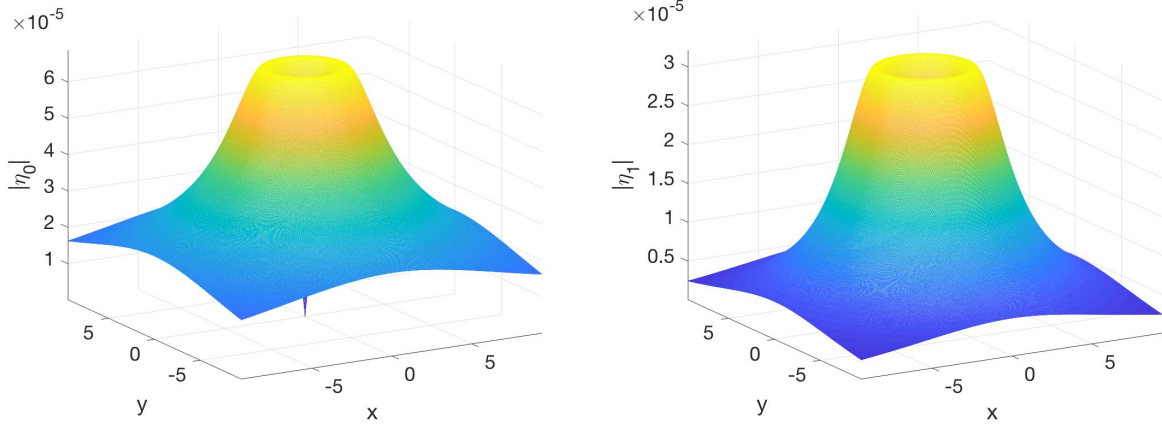


FIGURE 1. The modulus of the functions  $\eta_0$  (left) and  $\eta_1$  (right) of (16).

The singular integral is then computed via

$$(17) \quad \mathcal{F}^{-1} \left( \frac{S(\xi)}{\xi} \right) = \mathcal{F}^{-1} \left( \frac{S(\xi) - e^{-|\xi|^2} \sum_{n=0}^M \partial_{\bar{\xi}}^n S(0) \bar{\xi}^n / n!}{\xi} \right) + e^{-|\xi|^2} \sum_{n=0}^M \partial_{\bar{\xi}}^n S(0) (-2i\partial)^n \frac{i}{z} \left( 1 - e^{-\frac{|z|^2}{4}} \right).$$

Here the integer  $M$  is chosen so that the first term on the right hand side of the above equation is analytic within numerical precision, that is, its Fourier coefficients decrease to machine precision. The derivatives of  $S$  are again computed via Fourier techniques,

$$(18) \quad \partial_{\bar{\xi}}^n S(\xi) = \mathcal{F} [(-iz/2)^n \mathcal{F}^{-1} S].$$

Note that the derivatives are only needed for  $\xi = 0$ . To compute the first term on the right-hand-side of (17) at  $\xi = 0$ , we also need  $\partial_{\bar{\xi}} S(0)$  (according to L'Hopital's rule), which is computed as the derivatives in (18).

The second singular integral  $\mathcal{F}^{-1}[f(\xi)/(\bar{\xi} - 2ik)]$  will be computed in essentially the same way. Note that we have

$$\mathcal{F}^{-1} \left( \frac{e^{-|\xi|^2}}{\bar{\xi}} \right) = \frac{i}{\bar{z}} \left( 1 - e^{-\frac{|z|^2}{4}} \right),$$

and a standard Fourier shifting calculation yields

$$\mathcal{F}^{-1} \left( \frac{e^{-|\xi+2i\bar{k}/\epsilon|^2}}{\bar{\xi} - 2ik/\epsilon} \right) = e^{-(kz - \bar{k}\bar{z})/\epsilon} \frac{i}{\bar{z}} \left( 1 - e^{-|z|^2/4} \right),$$

along with

$$\mathcal{F}^{-1} \left( \frac{(\xi + 2i\bar{k}/\epsilon)^n e^{-|\xi+2i\bar{k}/\epsilon|^2}}{\bar{\xi} - 2ik/\epsilon} \right) = e^{-(kz - \bar{k}\bar{z})/\epsilon} (-2i\bar{\partial})^n \frac{i}{\bar{z}} \left( 1 - e^{-\frac{|z|^2}{4}} \right).$$

We compute

$$(19) \quad \mathcal{F}^{-1} \left( \frac{f(\xi)}{\bar{\xi} - 2ik/\epsilon} \right) = \mathcal{F}^{-1} \left( \frac{f(\xi) - e^{-|\xi + 2i\bar{k}/\epsilon|^2} \sum_{n=0}^M \partial_{\xi}^n f(-2i\bar{k}/\epsilon)/n! (\xi + 2i\bar{k}/\epsilon)^n}{\bar{\xi} - 2ik/\epsilon} \right) + e^{(\bar{k}\bar{z} - kz)/\epsilon} \sum_{n=0}^M \partial_{\xi}^n f(-2i\bar{k}/\epsilon)/n! (-2i\bar{\partial})^n \frac{i}{\bar{z}} \left( 1 - e^{-\frac{|z|^2}{4}} \right),$$

where we have used the shifting argument in Fourier space from (9). The derivatives of  $f$  are again computed via Fourier techniques,

$$(20) \quad \partial_{\xi}^n f(\xi) = \mathcal{F} [(-i\bar{z}/2)^n \mathcal{F}^{-1} f].$$

The above regularization procedure is only applied if  $2i\bar{k}/\epsilon$  is close to a  $\xi$  grid point which means that the minimum of  $|\xi + 2i\bar{k}/\epsilon|$  for  $\xi$  a grid point is smaller than the minimal distance between two points of this grid. If this is the case, we denote this grid point by  $\xi_0$  and apply the above formulae for  $\xi_0$  in place of  $-2i\bar{k}/\epsilon$ . The value of the first term of the right hand side of (19) at this  $\xi_0$  is then computed via  $\partial_{\xi} f(\xi_0)$  where the derivative is obtained with the same method as in (20).

**2.3. Numerical implementation.** The standard numerical approach to approximate Fourier transforms as in (13) is via discrete Fourier transforms which can be conveniently computed with a Fast Fourier transform (FFT). However, such methods will only be at their optimal efficiency when approximating periodic smooth functions. Functions in the Schwartz class are clearly not periodic, but when considered on a sufficiently large interval, they will have derivatives vanishing with the finite numerical precision at the boundaries of the computational interval. Thus the finite precision allows to approximate Schwartz class functions on such an interval as smooth periodic functions, and the coefficients of the FFT of the function will decrease exponentially as known for the standard Fourier transform of the function. Since also this implies that the numerical error decreases exponentially, such methods exhibit *spectral convergence*.

**Remark 2.3.** The problem of the D-bar system (7) is that singular Fourier multipliers appear which implies that the functions  $\Phi_{1,2}$  will not be in the Schwartz class, but have an algebraic decrease in  $z$  for  $|z| \rightarrow \infty$  in contrast to their derivatives. This is even a feature of crucial importance since the reflection coefficient (3) providing the scattering data in the context of the DS equation is given as the coefficient of the  $1/\bar{z}$  term near infinity. This apparent incompatibility of the D-bar solutions with an efficient setting for the application of FFT techniques is addressed in this paper in the following way: numerically only FFTs of smooth functions (within numerical precision) are computed, all other terms will be computed by hand as outlined in the previous subsection.

For the implementation we choose the computational domain

$$x \in L_x[-\pi, \pi], \quad y \in L_y[-\pi, \pi],$$

and the wave numbers in the FFT as

$$\xi_1 = (-N_x/2 + 1, -N_x/2 + 2, \dots, -N_x/2)/L_x, \quad \xi_2 = (-N_y/2 + 1, -N_y/2 + 2, \dots, -N_y/2)/L_y,$$

where  $N_x$  and  $N_y$  are the number of Fourier modes in the  $x$  and  $y$  direction respectively. As mentioned in remark 2.3, the values of  $L_x$ ,  $L_y$  and of  $N_x$  and  $N_y$  are chosen in a way that the Fourier transform of the studied Schwartz function decreases to machine precision as  $\xi_1$  and  $\xi_2$  approach the boundary of the computational domain. Since the derivatives of  $S$  in the regularization approach of the previous subsection are computed via (18) and (20), we want to ensure that also the inverse FFT of  $S$  decreases to machine precision ( $10^{-16}$  in our case, but in practice typically limited to  $10^{-14}$  because of rounding errors) to limit also the numerical errors in the computation of  $\mathcal{F}^{-1}S$  to this order. Thus we will show in the following examples that both the modulus of  $S$  and of  $\mathcal{F}^{-1}S$  decrease to machine precision for the chosen values of the parameters.

The small size of the functions  $\eta_n$ ,  $n = 0, 1, 2, \dots$  of (16) implies that in practice only a small number  $M$  of such functions is needed to compute the singular integrals to machine precision. For the examples studied in this paper,  $M = 4$  proved to be sufficient and is applied throughout all computations.

## 3. FIXED POINT ITERATION

The task to solve the D-bar system (7) with the asymptotic conditions (6) has been reduced in the previous section to the solution of the singular integral equation (13) and two singular quadratures (12) and (8). In this section we will solve the integral equation with a fixed point iteration and study the convergence of the iteration for several examples.

Thus we will solve equation (13) iteratively in the form

$$(21) \quad S^{(n+1)} = -\mathcal{F} \left[ q \mathcal{F}^{-1} \left( \frac{1}{\epsilon(\bar{\xi} - 2ik/\epsilon)} \mathcal{F} \left\{ \frac{\bar{q}}{\epsilon} \left( \mathcal{F}^{-1} \left( \frac{S^{(n)}}{\xi} \right) + 1 \right) \right\} \right) \right],$$

where  $n = 0, 1, 2, \dots$  and  $S^{(0)} = 0$ . The iteration is stopped once  $\|S^{(n+1)} - S^{(n)}\|_\infty$  is smaller than some threshold which is typically taken to be  $10^{-12}$ .

**Remark 3.1.** The computational cost per iteration without regularization is dominated by 4 2d FFTs. Per iteration there is a maximum of two regularizations for the singular integrals if  $2ik$  is close to a point of the  $\xi$  grid. Each of the regularizations requires an additional 2d FFT to compute the derivatives of the integrand. But since these derivatives are only computed at one single point, we compute the inverse FFT of the functions that need to be differentiated. The derivatives are then sums of this function multiplied with the respective powers of  $z$  or  $\bar{z}$  and an exponential factor. The main computational cost is thus 6 2d FFTs per iteration.

As concrete examples we will study in this paper the potentials

$$(22) \quad q = \exp(-x^2 - y^2),$$

$$(23) \quad q = \exp(-x^2 - 3xy - 5y^2),$$

i.e., a Gaussian and a rapidly decreasing potential which is not radially symmetric even asymptotically.

For the implementation we use  $N_x = N_y = 2^8$  Fourier modes and  $L_x = L_y = 3$ . Putting  $\Delta := \|S^{(n+1)} - S^{(n)}\|_\infty$ , one gets that the iteration converges linearly for  $k = 0$  and  $\epsilon = 1, 1/2$  for the examples (22), (23) as can be seen in Fig. 2 on the left. The residuals computed for equation (13) are  $1.69 * 10^{-11}$ ,  $6.71 * 10^{-12}$ ,  $1.11 * 10^{-12}$ ,  $8.39 * 10^{-13}$  as shown from left to right in the figure. It can be noted that the convergence becomes slower the smaller  $\epsilon$  is since this implies a potential  $q$  of larger  $L^\infty$  norm. Interestingly the convergence is slower for the symmetric (Gaussian) than for the non-symmetric potential. This can be seen on the right of Fig. 2 where the quantity  $\Delta$  is shown for the potential (23) and  $k = 0, 1$ ,  $\epsilon = 1/4$  (here we use  $N_x = N_y = 2^9$ ). Note that the iteration does not converge for the Gaussian potential for  $k = 0$  and  $\epsilon = 1/4$ . In order to have a convergent scheme, the  $L^\infty$  norm of the right hand side of (21), which is proportional to  $1/\epsilon^2$ , needs to be smaller than 1. On the other hand the iteration converges faster the larger  $|k|$  as can be seen from the right figure of Fig. 2. This is not surprising since a factor  $k$  appears in the denominator of equation (21), see [19] for a more detailed discussion of the large  $|k|$  limit.

The solution corresponding to the right figure of Fig. 2 can be seen in Fig. 3. Obviously the solutions tend only very slowly to the asymptotic values for  $|z| \rightarrow \infty$ . This comes again to show that it is only through the regularization approach we described in section 2 that Fourier methods can be used efficiently here.

Since only the quantity  $S$  is computed with FFT techniques, the numerical accuracy can be controlled as mentioned in remark 2.3 via the decrease of  $|S|$  with  $|\xi|$ . A logarithmic plot of  $|S|$  for the situation shown in Fig. 3 is presented on the left of Fig. 4. It can be seen that  $S$  decreases to machine precision. In order to control the numerical accuracy of the computation of the derivatives in (18) and (20) in the same way,  $\mathcal{F}^{-1}S$  also has to decrease to machine precision which is the case as shown on the right of Fig. 4.

The solution to the system (7) for the potential (23) and  $k = 1$ ,  $\epsilon = 1/4$ , for which the convergence was studied on the right of Fig. 2, can be seen in Fig. 5.

## 4. SOLUTION VIA GMRES

The fixed point iteration studied in the previous section converges without problems for potentials  $q$  with an  $L^\infty$  norm of order  $\epsilon$ . However this is no longer so for much larger  $L^\infty$  norms, in which case the iteration becomes computationally expensive or diverges or both. Since we are interested as in [2] in the semi-classical

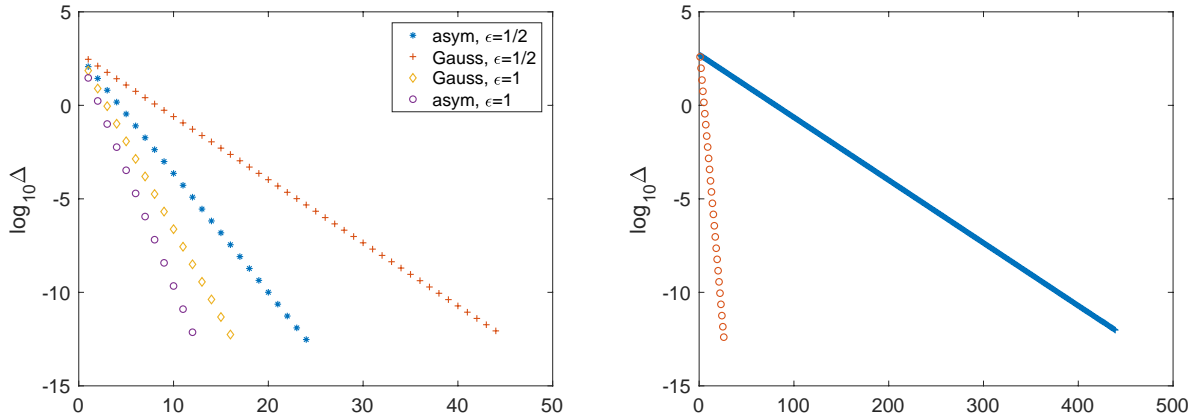


FIGURE 2. The quantity  $\Delta = \|S^{(n+1)} - S^{(n)}\|_\infty$  in a logarithmic plot for the iterative solution of (21) for the potentials (22) and (23) for  $k = 0$  and  $\epsilon = 1, 1/2$  on the left; on the right the same quantity for the potential (23),  $\epsilon = 1/4$  and  $k = 0$  ('+') and  $k = 1$  ('o').

limit  $\epsilon \ll 1$  (where  $q$  is essentially replaced by  $q/\epsilon$  in the equations with  $\epsilon = 1$ ), we present in this section an approach using GMRES. The fixed point iteration is mainly intended to provide a test of the accuracy of the GMRES approach to (13) and to compare the convergence of the latter with the fixed point iteration.

The basic idea of using GMRES is that an equation of the form  $Ax = b$ ,  $x, b \in \mathbb{R}^n$  and  $A$  an  $n \times n$  matrix, is solved iteratively by approaching  $A^{-1}b$  via linear combinations of  $b, Ab, \dots, A^N b$ . The convergence of this approach is not guaranteed, and often a *preconditioner* is needed, i.e., an  $n \times n$  matrix  $C$  such that the GMRES approach for  $(CA)x = Cb$  converges. We do not use preconditioners here. The comparison with the fixed point iteration is used to highlight possible advantages of GMRES.

An attractive feature of GMRES is that just the action of the matrix  $A$  on a given vector is needed, not the matrix itself, thus allowing to proceed just storing  $n$ -dimensional vectors instead of the  $n \times n$  matrix  $A$  thus reducing memory usage, a crucial advantage for the demanding problems studied here (note that the fixed point iterations has the same memory requirements as the GMRES approach). In our example, equation (13) is to be solved after an FFT discretisation. We put

$$(24) \quad b := \mathcal{F} \left[ q \mathcal{F}^{-1} \left( \frac{1}{\xi - 2ik/\epsilon} \mathcal{F} \{ \bar{q} \} \right) \right]$$

and

$$(25) \quad AS := \epsilon^2 S + \mathcal{F} \left[ q \mathcal{F}^{-1} \left( \frac{1}{\xi - 2ik/\epsilon} \mathcal{F} \left\{ \bar{q} \left( \mathcal{F}^{-1} \left( \frac{S}{\xi} \right) \right) \right\} \right) \right].$$

The matrix  $b$  is written as a vector by putting the columns one after the other to form a vector of length  $N_x N_y$ , and in an analogous way for  $AS$  (that is, column major ordering). Note that equation (13) has been multiplied by  $\epsilon^2$ . This has no influence on the convergence of GMRES since the euclidean norm of  $Ax - b$  divided by the euclidean norm of  $b$  controls the convergence. However, the absolute residuals which are limited by machine precision can be chosen similar in this case to what could be imposed for the fixed point iteration, see the discussion below.

We first study the situation of Fig. 5 with the same choice of the parameters, but this time with GMRES. The iteration is stopped here once the relative residual drops below  $10^{-14}$  which gives a residual of the same order as before. The difference between the solution with a fixed point iteration and the one with GMRES is shown in Fig. 6 on the left. It is obviously largest for small  $|\xi|$  (note that  $S$  is in the Schwartz class), but overall of the order of  $10^{-12}$  as expected.

The right figure of Fig. 6 shows the residuals  $\Delta_{\text{GMRES}}$  in dependence of the number of iterates for various values of  $\epsilon$  and  $k$ . It can be seen that for  $\epsilon = 1/4$ , the approach reaches maximal accuracy for



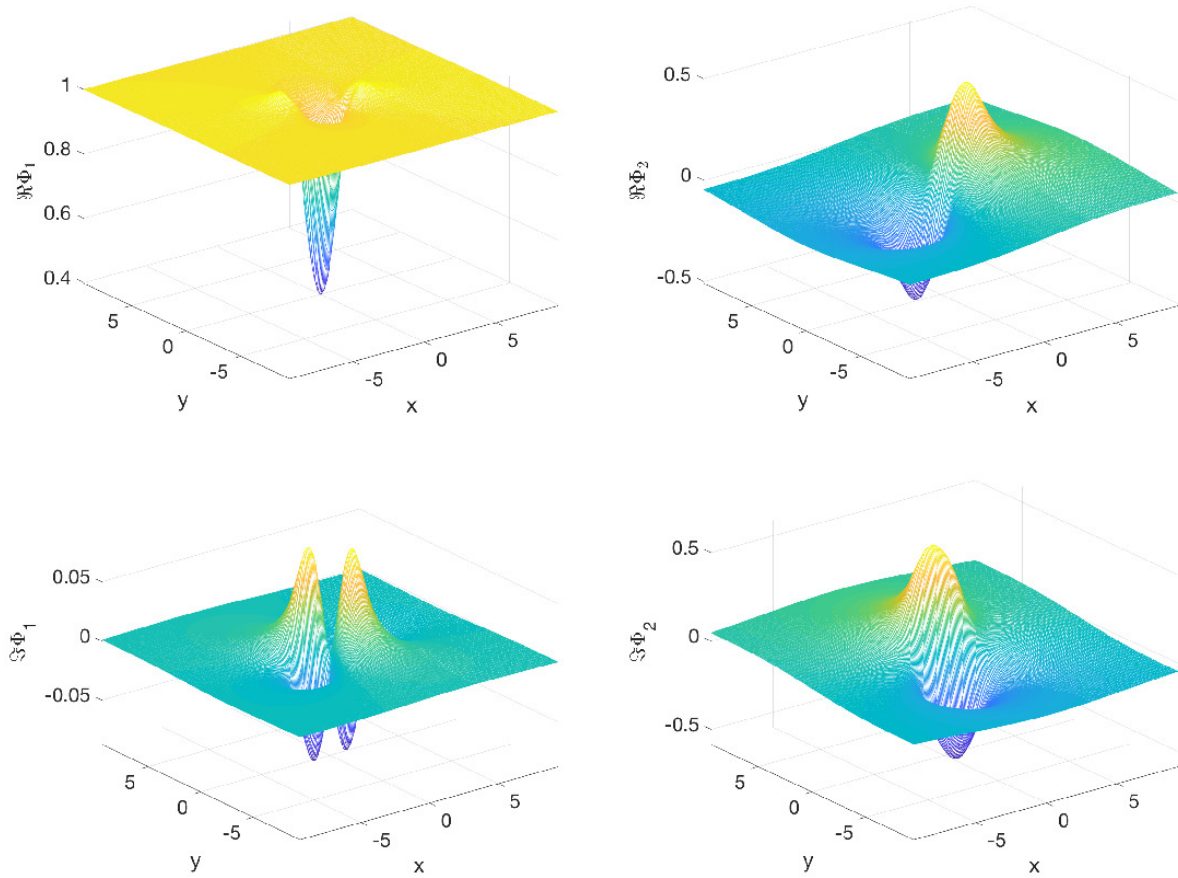


FIGURE 3. Solutions to the system (7) for the potential (23) for  $k = 0$  and  $\epsilon = 1/4$ , on the left  $\Phi_1$ , on the right  $\Phi_2$ , in the upper row the real parts, in the lower row the imaginary parts.

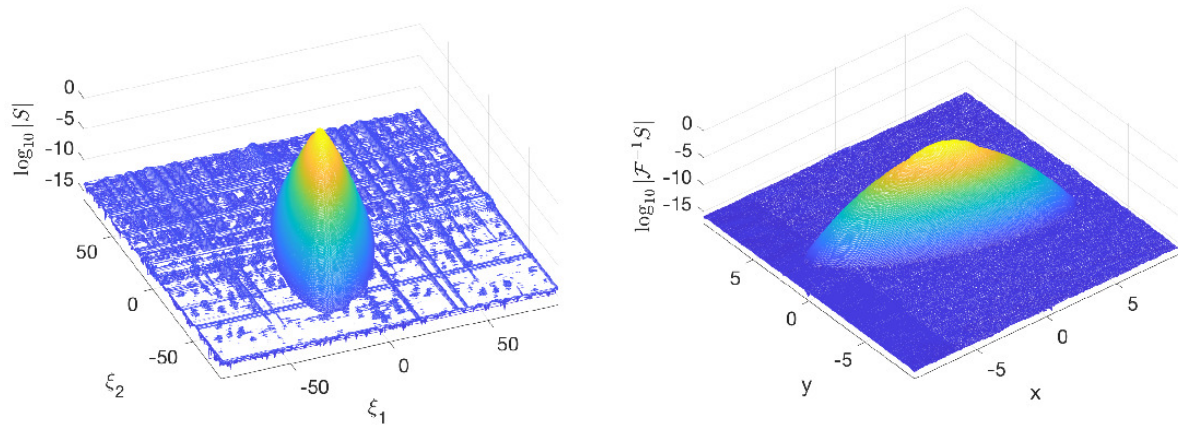


FIGURE 4. Solution to equation (13) for the potential (23) for  $k = 0$  and  $\epsilon = 1/4$  on the left, and its inverse Fourier transform on the right.

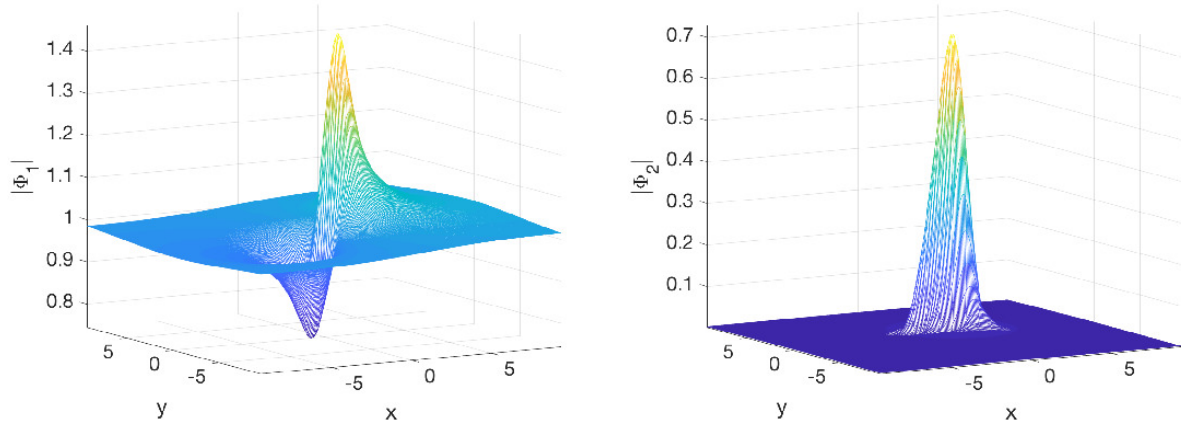


FIGURE 5. Solutions to the system (7) for the potential (23) for  $k = 1$  and  $\epsilon = 1/4$ , on the left  $\Phi_1$ , on the right  $\Phi_2$ .

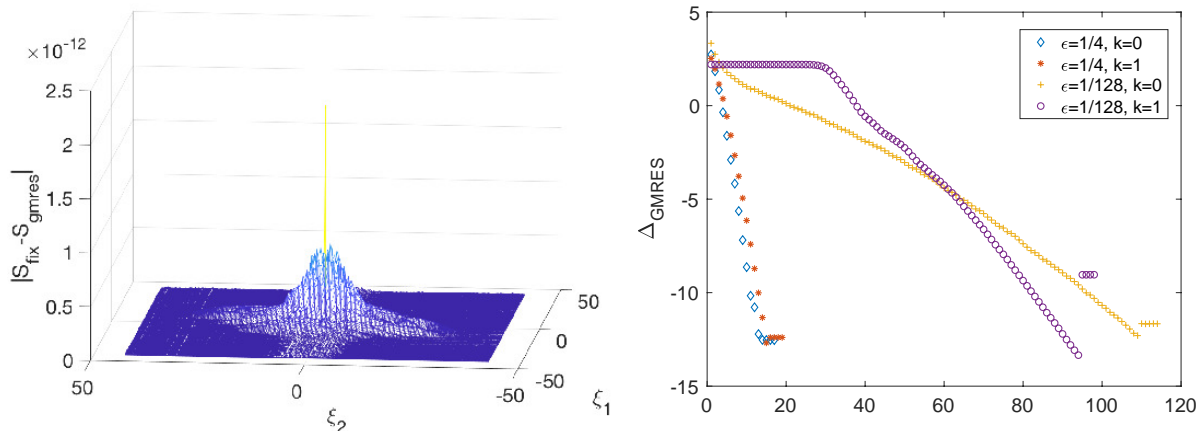


FIGURE 6. Difference of the solutions to the system (7) for the potential (23) for  $k = 1$  and  $\epsilon = 1/4$  obtained with a fixed point iteration and GMRES on the left, and on the right the residuals  $\Delta_{\text{GMRES}}$  for  $\epsilon = 1/4$ ,  $\epsilon = 1/128$  and  $k = 0, 1$ .

roughly 15 iterates which has to be compared to the corresponding figure on the right of Fig. 2 for the fixed point iteration. There for  $\epsilon = 1/4$  roughly 450 iterations were needed for  $k = 0$  and 40 for  $k = 1$ . This shows that GMRES is much more efficient in this case.

GMRES also allows to reach much smaller values of  $\epsilon$  than accessible with the fixed point iteration. We use  $L_x = L_y = 3$  and  $N_x = N_y = 2^{10}$  Fourier modes to study the solution for the potential (23) for  $\epsilon = 1/128$  and  $k = 0$ . The solutions can be seen in Fig. 7. Both solutions are clearly not radially symmetric, but are essentially constant in the vicinity of the origin. This is similar to the expected behavior for radially symmetric potentials discussed in [2]. GMRES converges after roughly 110 iterations as can be seen on the right of Fig. 6 when a plateau reached. The relative residual is of the order of  $10^{-15}$ , the residual of  $Ax - b$  with  $A, b$  of (25), (24) is of the order of  $10^{-13}$ .

The parameters for the computation are chosen in a way that both  $S$  and  $\mathcal{F}^{-1}S$  decrease to the level of the rounding error as can be seen in Fig. 8. Note that the latter is of the order of  $10^{-10}$  for the former since the maximum of  $|S|$  is of the order of  $10^4$  (in double precision it is in practice impossible to cover more than 14 orders of magnitude).

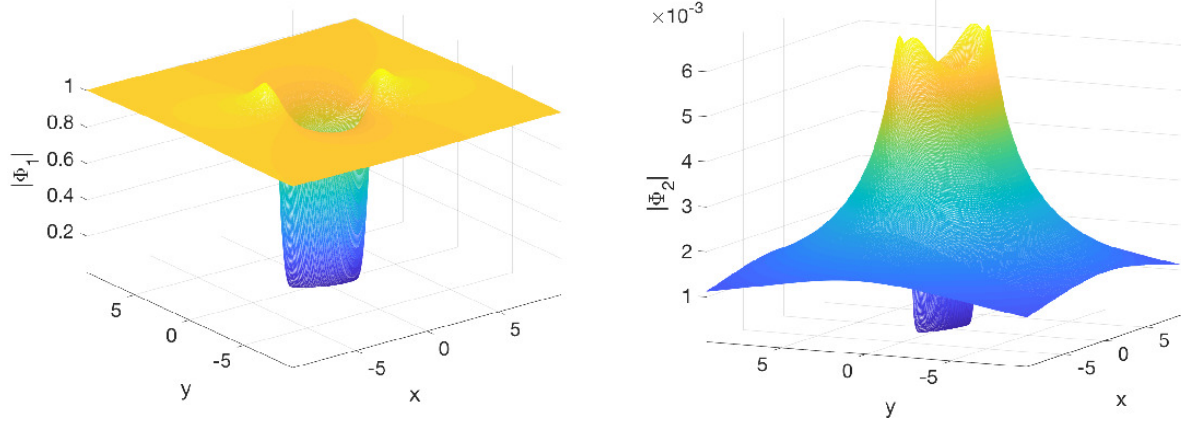


FIGURE 7. Solutions to the(13) for the potential (23)for  $k = 0$  and  $\epsilon = 1/128$  on the left  $\Phi_1$ , on the right  $\Phi_2$ .

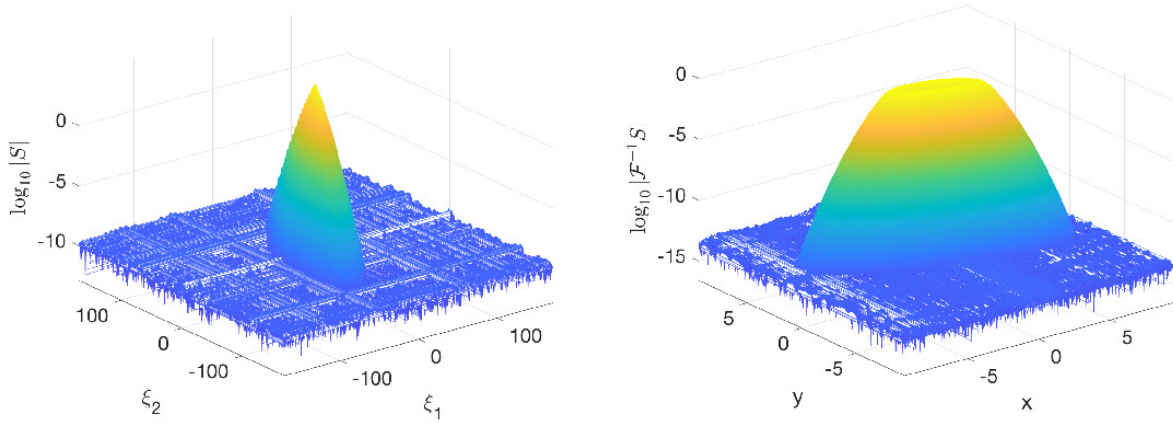


FIGURE 8. Solution  $S$  to the equation (13) for the potential (23) for  $k = 0$  and  $\epsilon = 1/128$  on the left and its inverse Fourier transform on the right.

To study the solution for the potential (23) for  $\epsilon = 1/128$  and  $k = 1$ , we use  $N_x = 2^9$  and  $N_y = 2^{10}$  Fourier modes and  $L_x = 2$ ,  $L_y = 1$ . The solution can be seen in Fig. 9. Note that the solution  $\Phi_1$  has a maximum of the order of  $10^4$ , but that the reflection coefficient being a rapidly decreasing function of the spectral parameter  $|k|$  is of the order of  $10^{-10}$  in this case. GMRES converges after roughly 90 iterations as can be seen on the right of Fig. 6. It stops since the last few iterations lead to a residual at a slightly higher plateau indicating that further iterations do not improve the accuracy. The residual of the equation is of the order of  $10^{-12}$  when the iteration is stopped.

The numerical parameters are chosen in a way that  $S$  and its inverse Fourier transform decrease to optimal precision. This can be seen on the left of Fig. 10. The function  $S$  decreases to the order of the saturation level which is here at around  $10^{-8}$  since the maximum of  $|S|$  is of the order of  $10^6$ . The inverse Fourier transform of  $S$  is shown on right of Fig. 10 to decrease to machine precision.

## 5. OUTLOOK

In this paper it was shown that CGO solutions to system (2) for potentials in the Schwartz class can be efficiently constructed via the integral equation (13) with FFT and iterative techniques. This can be done

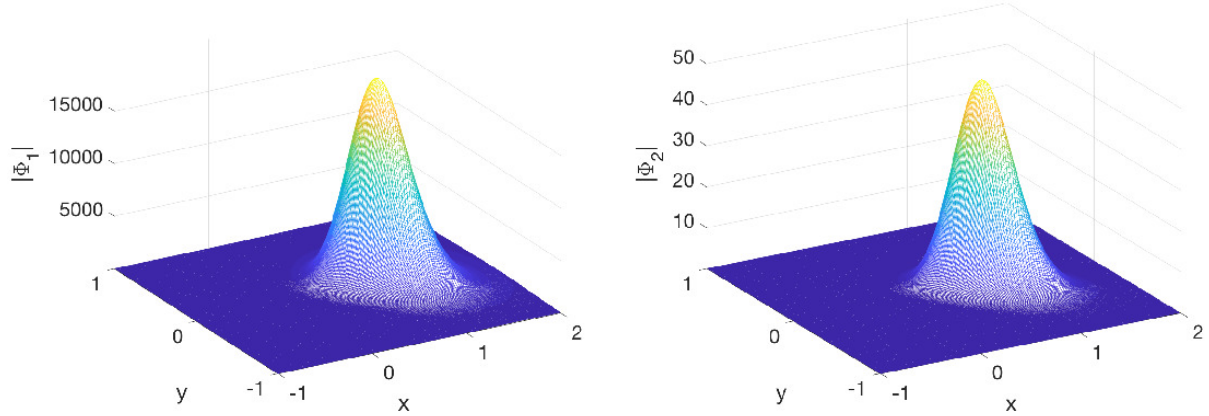


FIGURE 9. Solutions to the system (7) for the potential (23) for  $k = 1$  and  $\epsilon = 1/128$ ; on the left  $\Phi_1$ , on the right  $\Phi_2$ .

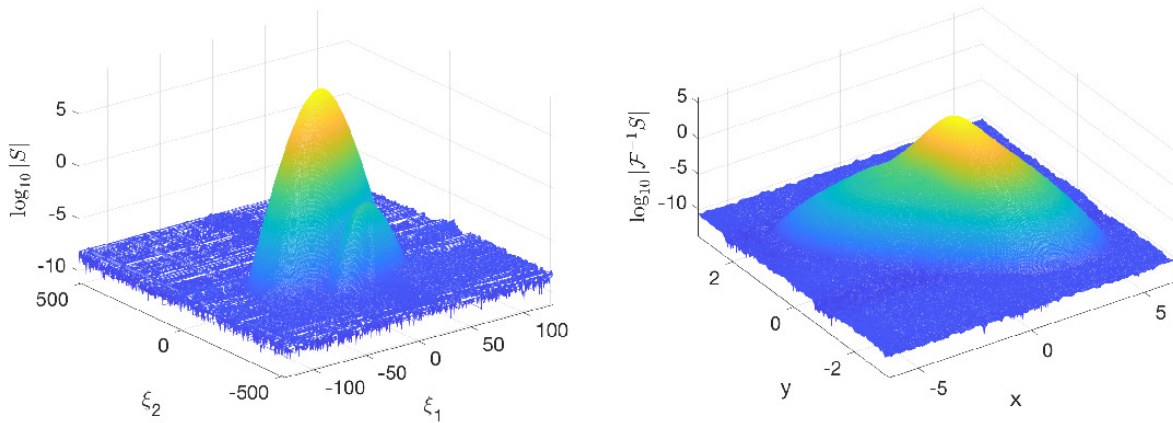


FIGURE 10. Solution to equation (13) for the potential (23) for  $k = 1$  and  $\epsilon = 1/128$  on the left, and its inverse Fourier transform on the right.

for a wide range of values of the spectral parameter  $k$  and for the semiclassical parameter  $\epsilon$ . The limiting factor for small  $\epsilon$  appears to be the conditioning of the matrix  $A$  in (25) which becomes worse the smaller  $\epsilon$  is. We could reach values of  $\epsilon = 1/256$ , but the achievable accuracy drops to the order of  $10^{-5}$  in this case.

This behavior is due to the singular character of the semiclassical solution which is discussed in [2]. There it is conjectured that the main contribution to the solution in this case to the CGO solutions is of the form  $\exp(f/\epsilon)$  where  $f$  solves an eikonal-type equation. It is not surprising that numerical approaches will ultimately fail to catch such a behavior for very small values of  $\epsilon$ . To address such questions, it appears best to use a *hybrid* approach, i.e., a combination of analytical and numerical techniques. In the present case this would mean to introduce functions  $\nu_i = e^{-f/\epsilon}\psi_i$ ,  $i = 1, 2$ , and solve numerically the system following from (2) for the functions  $\nu_{1,2}$  for a given solution  $f$  to the eikonal equation. This will be the subject of further work.

#### ACKNOWLEDGEMENT

This work was partially supported by the PARI and FEDER programs in 2016 and 2017, by the ANR-FWF project ANuI and by the Marie-Curie RISE network IPaDEGAN. K.M. was supported in part by

the National Science Foundation under grant DMS-1733967. We are grateful to J. Sjöstrand for helpful discussions and hints.

## REFERENCES

- [1] M. Ablowitz and R. Haberman. Nonlinear evolution equations in two and three dimensions. *Phys. Rev. Lett.*, 35:11858, 1975.
- [2] O. Assainova, C. Klein, K. McLaughlin and P. Miller, A Study of the Direct Spectral Transform for the Defocusing Davey-Stewartson II Equation in the Semiclassical Limit, <http://arxiv.org/abs/1710.03429>
- [3] R. Beals and R. Coifman, Multidimensional inverse scattering and nonlinear PDE Proc. Symp. Pure Math. (Providence: American Mathematical Society) vol 43 pp 45 - 70 (1985)
- [4] M. Bertola, A. Tovbis, Universality for the focusing nonlinear Schrödinger equation at the gradient catastrophe point: rational breathers and poles of the Tritronquée solution to Painlevé-I. *Comm. Pure Appl. Math.* 66 (2013), no. 5, 678-752.
- [5] J.C. Bronski, J.N Kutz, Numerical simulation of the semiclassical limit of the focusing nonlinear Schrödinger equation. *Phys. Lett.*, A 254 (2002) 325 - 336.
- [6] M. Cheney, D. Isaacson, and J. C. Newell. Electrical impedance tomography. *SIAM Review*, 41(1):85-101, 1999.
- [7] B. Dubrovin, T. Grava, C. Klein, On universality of critical behavior in the focusing nonlinear Schrödinger equation, elliptic umbilic catastrophe and the tritronquée solution to the Painlevé ?e-I equation. *J. Nonlinear Sci.* 19 (2009), no. 1, 57-94.
- [8] C. Klein and K. McLaughlin, Spectral approach to D-bar problems, *Comm. Pure Appl. Math.*, DOI: 10.1002/cpa.21684 (2017)
- [9] C. Klein and K. Roidot, Fourth order time-stepping for Kadomtsev-Petviashvili and Davey-Stewartson equations, *SIAM J. Sci. Comput.*, 33(6), 3333-3356. DOI: 10.1137/100816663 (2011).
- [10] C. Klein and K. Roidot, Numerical Study of the semiclassical limit of the Davey-Stewartson II equations, *Nonlinearity* 27, 2177-2214 (2014).
- [11] C. Klein and N. Stoilov, A numerical study of blow-up mechanisms for Davey-Stewartson II systems, *Stud. Appl. Math.*, DOI : 10.1111/sapm.12214 (2018)
- [12] S. Jin, C.D. Levermore, D.W. McLaughlin, The semiclassical limit of the defocusing NLS hierarchy. *Comm. Pure Appl. Math.* 52 (1999) 613654.
- [13] K. Knudsen, J. L. Mueller, S. Siltanen. Numerical solution method for the d-bar equation in the plane. *J. Comput. Phys.* **198** no. 2, 500-517 (2004).
- [14] J.L. Mueller and S. Siltanen. *Linear and Nonlinear Inverse Problems with Practical Applications*, SIAM, 2012.
- [15] A. I. Nachman, I. Regev, and D. I. Tataru, A nonlinear Plancherel theorem with applications to global well-posedness for the defocusing Davey-Stewartson equation and to the inverse boundary value problem of Calderon, arXiv:1708.04759, 2017.
- [16] P. Perry. Global well-posedness and long-time asymptotics for the defocussing Davey-Stewartson II equation in  $H^{1,1}(\mathbb{R}^2)$ . Preprint available at [arxiv.org/pdf/1110.5589v2.pdf](https://arxiv.org/pdf/1110.5589v2.pdf).
- [17] Y. Saad and M. Schultz, *GMRES: A generalized minimal residual algorithm for solving nonsymmetric linear systems*. *SIAM J. Sci. Comput.* **7** (1986), no. 3, 856-869.
- [18] E.I. Schulman, On the integrability of equations of Davey-Stewartson type, *Theor. Math. Phys.* 56 (1983), 131-136.
- [19] J. Sjöstrand, *private communication*.
- [20] Trefethen, L.N.: *Spectral Methods in Matlab*. SIAM, Philadelphia (2000)
- [21] G. Uhlmann. Electrical impedance tomography and Calderón’s problem. *Inverse Problems*, 25(12):123011, 2009.

(C. Klein) INSTITUT DE MATHÉMATIQUES DE BOURGOGNE 9 AVENUE ALAIN SAVARY, BP 47870, 21078 DIJON CEDEX  
*E-mail address:* christian.klein@u-bourgogne.fr

(K. McLaughlin) DEPARTMENT OF MATHEMATICS, 1874 CAMPUS DELIVERY, FORT COLLINS, CO 80523-1874  
*E-mail address:* kenmcl@rams.colostate.edu

(N. Stoilov) INSTITUT DE MATHÉMATIQUES DE BOURGOGNE, UMR 5584, UNIVERSITÉ DE BOURGOGNE-FRANCHE-COMTÉ, 9 AVENUE ALAIN SAVARY, 21078 DIJON CEDEX, FRANCE  
*E-mail address:* Nikola.Stoilov@u-bourgogne.fr